Room-Temperature Strong Coupling between CdSe Nanoplatelets and a Metal–DBR Fabry–Pérot Cavity

Ovishek Morshed,[1] Mitesh Amin,[1] Nicole M. B. Cogan,[2] Eric R. Koessler,[2] Robert Collison,[1] Trevor M. Tumiel,[2] William Girten,[2] Farwa Awan,[2] Lele Mathis,[3] Pengfei Huo,[2,1] A. Nickolas Vamivakas,[1,4] Teri W. Odom,[5,3] and Todd D. Krauss[2,1]

[1)]*The Institute of Optics, University of Rochester, Rochester, New York 14627, USA.*

[2)]*Department of Chemistry, University of Rochester, Rochester, New York 14627, USA.*

[3)]*Department of Materials Science and Engineering, Northwestern University, Evanston, Illinois 60208, USA.*

[4)]*Department of Physics and Astronomy, University of Rochester, Rochester, New York 14627, USA.*

[5)]*Department of Chemistry, Northwestern University, Evanston, Illinois 60208, USA.*

(*Electronic mail: todd.krauss@rochester.edu)

(Dated: 26 March 2024)

The generation of exciton–polaritons through strong light–matter interactions represents an emerging platform for exploring quantum phenomena in molecular systems. A significant challenge in molecular polaritonic systems is the ability to operate at room temperature with high fidelity. Here, we demonstrate the generation of room-temperature exciton–polaritons through the coupling of CdSe nanoplatelets (NPLs) with a Fabry–Pérot optical cavity, leading to a Rabi splitting of 74.6 meV. Quantum-classical calculations accurately predict the complex dynamics between the many dark state excitons and the optically allowed polariton states, including the experimentally observed lower polariton photoluminescence emission, and the concentration of lower polariton photoluminescence intensities at higher in-plane momenta as the cavity becomes more negatively detuned. The Rabi splitting measured at 5 K is similar to that at 300 K, validating the feasibility of the temperature-independent operation of this polaritonic system. Overall, these results show that CdSe NPLs are an excellent material to facilitate the development of room-temperature quantum technologies.

I. INTRODUCTION

Exciton–polaritons, generated from the strong coupling between electronic states of molecules and photons confined within an optical cavity, have drawn significant interest for applications in a number of different fields including polariton chemistry, quantum electrodynamics, quantum computing, and quantum simulations.[1–6] However, due to rapid decoherence,[7] the strongly-coupled light–matter states that are necessary for these applications often exist at cryogenic temperatures,[8–10] which limits their practical utility. Therefore, for widespread use of exciton–polaritons in future technologies, it is imperative to achieve strong light–matter coupling in a robust system that can be actively controlled at room temperature.[1,10–12]

Incorporating solution-processed active materials into exciton–polariton systems has advantages due to their low-cost synthesis and facile ability to integrate into devices for room-temperature operation.[3,13,14] Indeed, recently, there has been an active interest in investigating novel, solution-processable polaritonic systems displaying interesting physical characteristics at ambient temperatures.[2] For example, polariton Bose–Einstein condensates have been observed in lead-halide perovskite nanowire microcavities.[13] In dielectric Fabry–Pérot optical cavities containing a thin film of lead-halide perovskites, strong polariton–polariton scattering was observed.[15] Colloidal quantum dots (QDs) have also drawn significant attention as a well-investigated system for exploring strong light–matter coupling within optical cavities.[16–18] For instance, strong coupling has been demonstrated by integrating colloidal QDs into a high-Q microcavity, resulting in a Rabi splitting of 24 – 32 meV,[19] a phenomenon observed even with single QDs in a Fabry–Pérot cavity at room temperature.[20] However, limited oscillator strength[21] and comparatively broad fluorescence linewidth[3] of these QDs present challenges in achieving substantial Rabi splitting in such systems.

Cadmium selenide (CdSe) nanoplatelets (NPLs) are a class of solution-processable materials that are promising for studies of strong light–matter interactions.[22–27] Much like two-dimensional (2D) semiconductor quantum wells, NPLs demonstrate strong quantum confinement along the longitudinal (*i.e.* shortest) dimension[28] with an in-plane transition dipole moment[29] and an exceptionally large oscillator strength.[30] Thus, on a per-particle basis, NPL excitons should more easily couple to the photonic states of an optical cavity. In addition, NPLs have a well-defined thickness that leads to homogeneously broadened linewidths along with a substantial exciton-binding energy,[3,22–25,31,32] offering advantages for achieving strong light–matter coupling at room temperature given the relatively large thermal excitation energy at 300 K.[33] However, like other solution-processable cavity–matter systems, incorporating NPLs into optical cavities poses challenges associated with sample preparation, including obtaining high-quality optical films of a dense array of NPLs.[32]

In this work, we show that strong coupling between CdSe NPLs and the optical field of a Fabry–Pérot cavity can be achieved at room temperature (300 K). The optical cavity consists of a pure NPL layer deposited between a dielectric and a metal mirror. A Fourier-space imaging system was used to

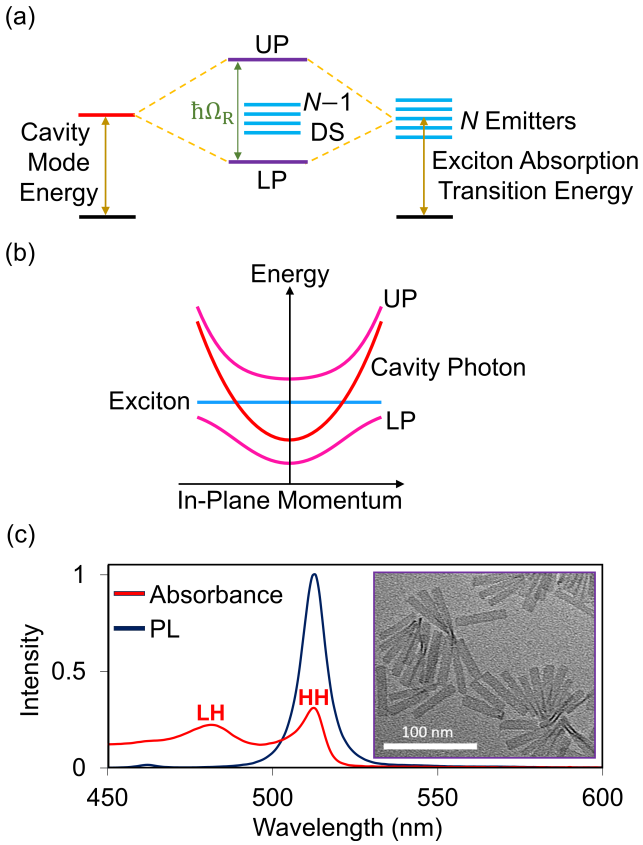

FIG. 1. (a) Energy level diagram depicting the resonance interaction between a two-level system and a confined electromagnetic field within an optical cavity. DS, UP, and LP represent the dense manifold of dark exciton states, upper polariton states, and lower polariton states, respectively. (b) Energy–momentum dispersion characteristics of the upper and the lower polariton states, showing the energy anti-crossing behavior. (c) Absorption and PL spectra of the synthesized 4.5 ML CdSe NPLs in hexane. A TEM image of these NPLs is shown in the inset.

provide insights into the photophysical properties of polaritons as a function of in-plane momenta and to characterize the strength of light–matter coupling.[32] The NPL–cavity system was found to be in the collective strong coupling regime with a Rabi splitting of 74.6 meV at room temperature, confirmed by the angle-resolved reflectance and photoluminescence (PL) measurements. Quantum dynamics simulations including cavity loss, phonon-assisted non-adiabatic coupling between polaritons and excitons, and multiple cavity modes, accurately reproduce the observed PL properties of the exciton–polaritons. Overall, the discovery of a facile system that exhibits strong light–matter coupling in ambient conditions should provide significant insights into the rich population dynamics of polaritons and thus enable groundbreaking advancements in polariton chemistry.[34]

II. FORMATION OF EXCITON–POLARITONS

For a planar Fabry–Pérot cavity structure, the cavity photon field is confined in the z-direction and the energy–momentum relationship of the photon can be expressed as

$$E_{\mathrm{ph}}(\theta) = \frac{\hbar c}{n_{\mathrm{e}}} k = \frac{\hbar c}{n_{\mathrm{e}}} \sqrt{k_{\perp}^2 + k_{\parallel}^2}, \tag{1}$$

where $k_{\parallel} = \sqrt{k_x^2 + k_y^2}$ represents the in-plane wavevector, $k_{\perp}$ represents the out-of-plane wavevector in the direction of the confined field, c is the speed of light, and n_{e} is the effective refractive index of the cavity. The relationship between the in-plane and the out-of-plane wavevector can be expressed as $\tan\theta = k_{\parallel}/k_{\perp}$ where θ corresponds to the angle relative to the z-direction. Accordingly, the cavity photon energy can be expressed as

$$E_{\mathrm{ph}}(\theta) = \frac{\hbar c}{n_{\mathrm{e}}} k_{\perp} \sqrt{1 + \tan^2\theta}. \tag{2}$$

For small angles (θ), the photon energy can be approximated as

$$E_{\mathrm{ph}}(\theta) \approx \frac{\hbar c}{n_{\mathrm{e}}} k_{\perp} (1 + \frac{1}{2}\tan^2\theta). \tag{3}$$

Eq. (3) shows that the dispersion of the cavity photon mode is parabolic for a small angular range.

In the strong exciton–photon coupling regime, two new light–matter hybrid eigenstates (*i.e.* polaritons) are created with an energy separation given by the Rabi splitting energy,[33,35] as illustrated in Fig. 1a. When considering the spectral dispersion of the NPL excitons and the Fabry–Pérot cavity modes, strong light–matter coupling manifests as an avoided crossing between the coupled modes,[36] as shown in Fig. 1b. Thus, including momentum-related dispersion, strong light–matter coupling produces an upper polariton (UP) and a lower polariton (LP) branch, which have a relative admixture of excitonic and photonic properties.[37,38] According to the Tavis–Cummings model,[39] the eigenenergies corresponding to UP (E_+) and LP (E_-) under the collective light–matter coupling regime can be expressed as

$$\begin{aligned} E_{\pm}(\theta) = & \frac{1}{2}\left[E_{\mathrm{x}} + \hbar\omega_{\mathrm{c}}(1 + \frac{1}{2}\tan^2\theta)\right] \\ & \pm \frac{1}{2}\sqrt{\left[\hbar\omega_{\mathrm{c}}(1 + \frac{1}{2}\tan^2\theta) - E_{\mathrm{x}}\right]^2 + 4Ng_{\mathrm{c}}^2}, \end{aligned} \tag{4}$$

where $\omega_{\mathrm{c}} = ck_{\perp}/n_{\mathrm{e}}$ is the frequency of the cavity photon in the z-direction, E_{x} is the exciton energy, g_{c} is the light–matter coupling strength, and N is the total number of coupled emitters. The light–matter detuning is defined as

$$\Delta E(\theta) = \hbar\omega_{\mathrm{c}}(1 + \frac{1}{2}\tan^2\theta) - E_{\mathrm{x}}. \tag{5}$$

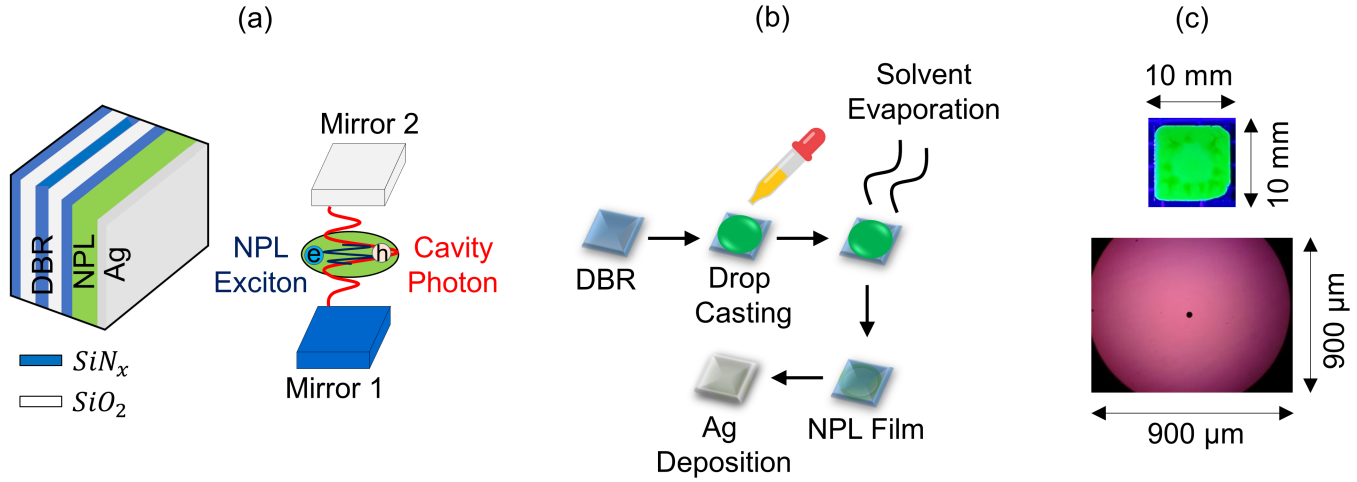

FIG. 2. (a) Schematic of the DBR–Metal hybrid cavity structure. The DBR consists of 15.5 pairs of alternating layers of SiN_x and SiO_2, among which only 2.5 pairs are shown. The interaction between the NPL excitonic oscillations and the electromagnetic field of the cavity photons is also illustrated. (b) Solid-state film deposition from a colloidal NPL solution to fabricate a Fabry–Pérot cavity with a bottom-up approach. (c) Uniform NPL films where the top panel corresponds to the deposited film on a 10 mm × 10 mm DBR substrate under UV illumination and the bottom panel is an optical microscope (10X objective) image on a 900 μm × 900 μm scale, captured with a Filmetrics F20 imaging system.

For a specific incident angle (θ_0), resonance occurs where the light–matter detuning $\Delta E(\theta_0)$ becomes zero. At resonance, the energy difference between $E_+(\theta_0)$ and $E_-(\theta_0)$ becomes

$$\hbar\Omega_R = E_+(\theta_0) - E_-(\theta_0) = 2\sqrt{N}g_c. \quad (6)$$

This energetic separation between UP and LP is commonly referred to as the *vacuum Rabi splitting*.[40] For N emitters in the collective coupling regime, there is also a manifold of N–1 *dark states* with nearly zero transition dipole[34] which represent exciton modes that do not couple to the cavity. Eq. (6) shows that Rabi splitting is proportional to $\sqrt{N}$, *i.e.* the more NPLs effectively couple to the cavity, the larger the Rabi splitting. To fulfill the strong coupling criterion, where the coherent energy exchange rate between light and matter exceeds their individual decay rates, the Rabi splitting energy ($\hbar\Omega_R$) must be larger than the energies corresponding to the combined decay rates of photons ($\hbar\gamma_c$) and excitons ($\hbar\gamma_x$).

III. SAMPLE FABRICATION

The synthesis of CdSe NPLs was adapted from recently developed procedures.[22,41] The absorption and PL spectra of these NPLs are presented in Fig. 1c. The NPLs exhibit two well-defined peaks in absorption at 512 nm (2.422 eV) and 481 nm (2.578 eV), corresponding to the heavy-hole (HH) and the light-hole (LH) exciton transitions, respectively. The PL maximum is at 513 nm (2.417 eV) with a full-width half-maximum (FWHM) of 9.5 nm (≈ 45 meV), resulting in a very small (≈ 4.7 meV) *Stokes shift*. The average lateral dimension of the NPLs was estimated from the transmission electron microscope (TEM) image as 38.8 ± 3.7 nm × 7 ± 1.1 nm with a thickness ≈ 1.2 nm, corresponding to 4.5 monolayers (MLs).

The cavity consists of a thin film of 4.5 ML CdSe NPLs in between two highly reflective mirrors. A schematic of the cavity structure is presented in Fig. 2a. The bottom mirror is a *distributed Bragg reflector* (DBR) while the top mirror is a 40 nm thick metal (Ag) layer. The NPL film was prepared by drop-casting concentrated NPLs in hexane on top of the DBR substrate, as illustrated in Fig. 2b (see *Supplementary Information* for more details). As shown in Fig. 2c, the resulting NPL film is optically smooth, which is critical for high-quality cavity operation with minimal loss. The quality factor, Q, of the cavity, is estimated as $\hbar\omega_c/\hbar\gamma_c$ where $\hbar\omega_c$ is the energy of the cavity mode calculated from the central linecut of the angle-resolved reflectance from a highly red-detuned cavity (*i.e.* a polariton with mostly photonic character). Assuming the polariton reflectance linewidth corresponds to the cavity decay rate $\hbar\gamma_c$, we calculate $Q \approx 60$ (Fig. S4a) for this NPL–cavity system.

IV. EXPERIMENTAL RESULTS

Polariton photophysical properties are characterized by measuring angle-resolved reflectance and PL spectra. This measurement was performed using a Fourier-space spectroscopy system where the back focal plane of the microscope objective was relayed to the entrance slit of a spectrometer through a tube lens, thus effectively mapping incident angles into spatial positions.[32] The range of collection angles, defined by the effective refractive index of the cavity and the numerical aperture of the microscope objective used in the Fourier imaging system, is calculated to be ± 20°. Further information on the experimental setup is available in the *Supplementary Information*.

Fig. 3a presents the angle-resolved reflectance spectrum for an NPL-filled cavity at room temperature where the sample

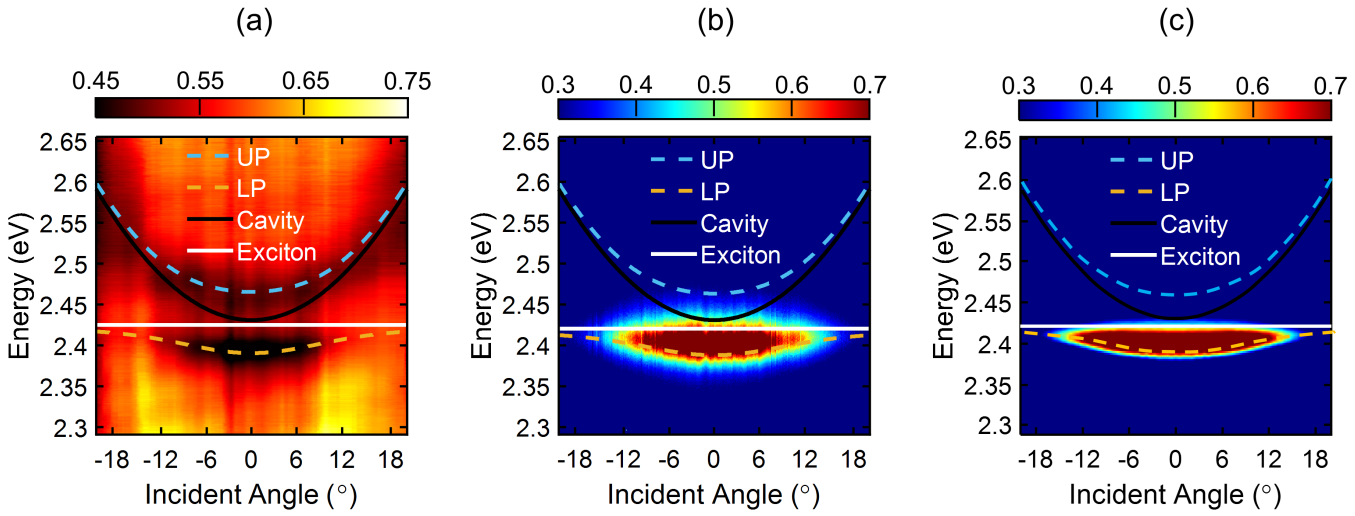

FIG. 3. Angle-resolved measurements from the NPL–cavity hybrid system at T = 300 K. (a) Angle-resolved white light reflectance spectrum showing both the UP and the LP branches. The solid lines show exciton and cavity dispersions whereas the dashed lines represent polariton dispersions fitted using the coupled harmonic oscillator model. (b) Angle-resolved PL spectrum showing only the LP emission. The white solid line is shown at a slightly lower energy (4.7 meV) than that in the reflectance spectrum to represent the Stokes shift. (c) Angle-resolved PL spectrum obtained from theoretical simulations (see Appendix for details).

was illuminated by a broadband white light source. The spectrum clearly shows two separated branches corresponding to the upper and the lower polaritons. As the collection angle increases, the LP branch deviates from following the cavity photon dispersion and instead follows the flat exciton dispersion, and *vice-versa* for the UP branch. The two polariton branches can be fitted to $E_+(\theta)$ and $E_-(\theta)$ given by the coupled harmonic oscillator model in Eq. (4). The collective coupling strength is estimated to be $\sqrt{N}g_c = 37.3$ meV, corresponding to a room-temperature Rabi splitting, $\hbar\Omega_R = 74.6$ meV at resonance (*i.e.* when cavity–exciton detuning, $\Delta E(\theta) = 0$). The Rabi splitting extracted from our NPL-filled cavity system satisfies the strong coupling criterion as

$$\hbar\Omega_R > \sqrt{(\hbar\gamma_c)^2 + (\hbar\gamma_x)^2} = 54.1\ meV, \tag{7}$$

where $\hbar\gamma_x$ is the linewidth corresponding to the exciton dephasing rate, estimated to be 38.2 meV from the FWHM linewidth of single NPL PL spectrum at 300 K, and $\hbar\gamma_c$ is the linewidth of the cavity photons, estimated to be 38.3 meV from the central linecut of the reflection spectrum obtained from a reference red-detuned cavity.

For this particular cavity, the energy of the cavity mode is slightly larger than the energy of the heavy-hole exciton at normal incidence (*i.e.* at $\theta = 0^o$), resulting in a slightly positively detuned cavity with $\Delta E = 5.9$ meV. Here, the UP branch dominates the reflection spectrum across the whole range of collection angles whereas the LP branch loses signal intensity at higher angles. The lack of reflectivity occurs due to the negligible photonic character of LP dictated by the *Hopfield coefficients* that describe the degree of exciton–photon mixing in the coupled modes.[42] As the collection angle slightly increases, cavity–exciton detuning becomes exactly zero, indicating the two modes approach resonance.[43] Consequently, two symmetric equal-intensity reflectivity dips are observed (Fig. S4b).

The large oscillator strength of the NPLs offers the advantage of requiring fewer molecules to achieve a substantial Rabi splitting compared to small molecule organic chromophores. The number of NPLs effectively coupled to the cavity can be estimated[26,32] as

$$\hbar\Omega_R = 2\sqrt{N}g_c = \mu_{eg}\sqrt{N}\sqrt{\frac{2\hbar\omega_c}{\varepsilon_0 n_e^2 \mathscr{V}}}. \tag{8}$$

Here, $\mu_{eg} \approx 18$ Debye is the ground-to-excited state transition dipole moment of an individual NPL,[44] $\hbar\omega_c$ is the energy of the cavity mode, ε_0 is the vacuum permittivity, $n_e \approx 1.7$ is the effective refractive index of the cavity, and $\mathscr{V}$ is the mode volume of the cavity, which is estimated by treating the cavity thickness as the Rayleigh distance of the cavity mode.[32] Using Eq. (8), it was found that approximately $N \approx 12,200$ NPL molecules are effectively coupled to the cavity. This number is significantly smaller than the typical number of emitters ($N = 10^6 - 10^{10}$) involved in most polaritonic chemistry experiments.[45,46]

The angle-resolved PL spectrum of the cavity sample is shown in Fig. 3b. The PL spectrum demonstrates that polariton emission predominantly occurs within the LP branch. Notably, emission from the UP branch is not observed. The predominance of the LP emission in the PL spectrum is supported by theoretical simulations[47,48] of the angle-resolved PL, shown in Fig. 3c. The PL spectrum was calculated based on the population dynamics of the generalized Holstein–Tavis–Cummings (GHTC) model in the presence of cavity loss, which has recently been used to describe the angle-resolved spectra and the dynamics of strongly coupled

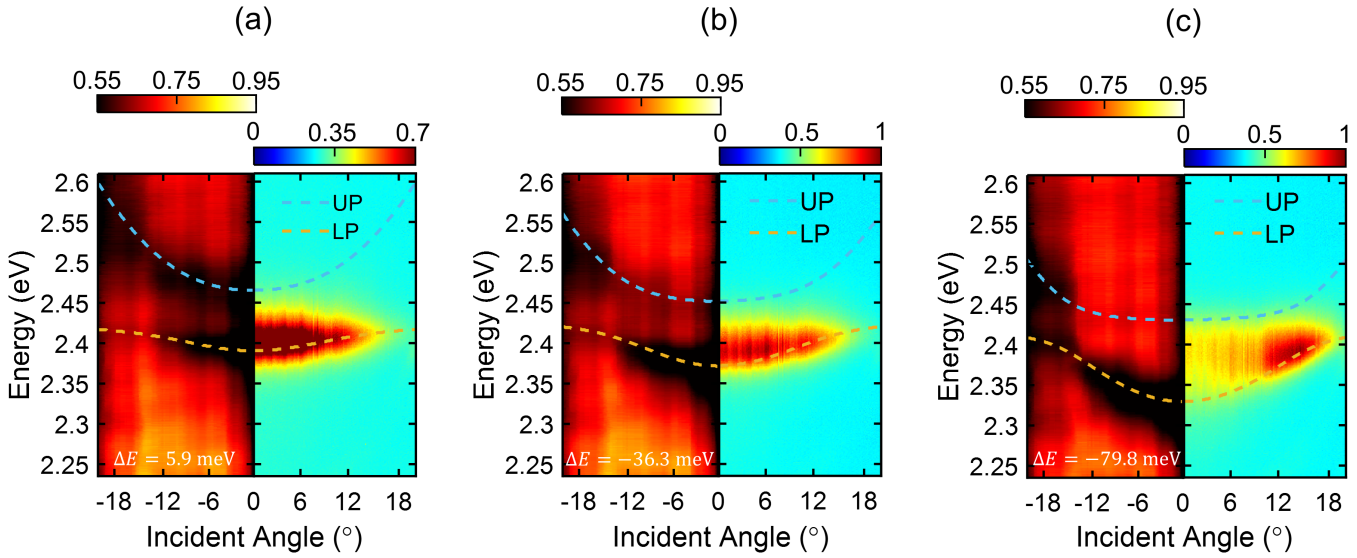

FIG. 4. Angle-resolved measurements for three different cavities with varied detunings at T = 300 K. The left panels of each figure correspond to the angle-resolved reflectance spectra whereas the right panels correspond to the PL spectra. The cavity–exciton detunings at normal incidence are (a) $\Delta E = 5.9$ meV, (b) $\Delta E = -36.3$ meV, and (c) $\Delta E = -79.8$ meV, respectively. All three cavities have similar Rabi splitting, $\hbar\Omega_R \approx 70 - 75$ meV.

systems.[49–52] The simulated PL spectrum shows greater PL intensity at smaller angles for energies slightly blue-detuned from the LP dispersion, with decreasing PL intensity at larger angles and energies above the exciton energy. These features are an excellent match to those of the measured PL spectra (Fig. 3b), demonstrating the ability of the model to accurately describe exciton–polariton systems.

Importantly, the excellent agreement between theory and experiment allows for insights into the physical origins of the observed angle-resolved spectra, and in particular, the role of the dark states exciton manifold. In agreement with other recent studies,[53–61] we find that the dark states in this NPL–cavity system essentially act as a population reservoir that cycles excited exciton population among the polariton states. In the absence of intermolecular interactions, the polaritons remain decoupled from the dark states manifold. However, the dark states can acquire oscillator strength from the bright polaritons through vibronic coupling, which modifies polariton dispersion characteristics.[54,62] PL from the UP is not observed, since the decay from UP to dark states is much faster compared to that from dark states to LP due to the large density of states of the dark state reservoir.[63] The redistribution of population from UP and LP states toward the reservoir of dark states also results in blue-shifted LP emission compared to absorption.[54,64,65]

Fig. 4 shows angle-resolved reflectance and PL measurements for three different cavities with varied detunings at ambient temperature. A Rabi splitting of 70 – 75 meV is observed for all three systems, showing that the coupling strength is independent of cavity–exciton detuning. This independence with respect to detuning is expected since the number of emitters as well as the cavity mode volume hardly changes with the slight cavity thickness variations that cause the detuning values in Fig. 4. However, as the cavity becomes more negatively detuned, meaning the heavy-hole exciton increasingly deviates (to higher energies) from the resonance condition, the phase relationship between the exciton and the cavity mode's oscillations starts to become less favorable for coherent interaction. As illustrated in Fig. 4a–c, the LP branch tends to have more curvature as the cavity detuning shifts from 5.9 meV to −79.8 meV. With large detuning, the LP PL intensity tends to become stronger at higher angles, corresponding to higher in-plane momenta, which has been observed in our previous system.[32] This phenomenon is commonly referred to as the *bottleneck effect*,[66] characterized by the accumulation of polaritons within a bottleneck-like region. In this case, the PL intensity becomes weaker at small angles where the LP branch is not significantly populated. The diminished excitonic nature along with the enhanced photonic character of LP results in a decrease in the exciton–phonon scattering rate which contributes toward the depletion of the polariton population in the region of lower in-plane momenta with mostly photon-like characteristics.[66,67]

In contrast to the behavior of LP, as the cavity is tuned to smaller energies, the intensity of the UP branch diminishes in the reflectance spectrum at small angles owing to negligible photonic character. The larger the detuning, the more the excitonic character of UP increases at these small angles, resulting in the congregation of reflectance signals (*i.e.* UP absorbance intensities) at higher angles. The PL blue-shifting becomes more evident as the cavity becomes more red-detuned, rendering increased photonic character to the LP branch which enables the dark states to borrow significant photonic character from the bright LP state.[54] The transfer of population from UP and LP to the dark states enhances the repulsive interaction between polaritons, which has been reported[68,69] to

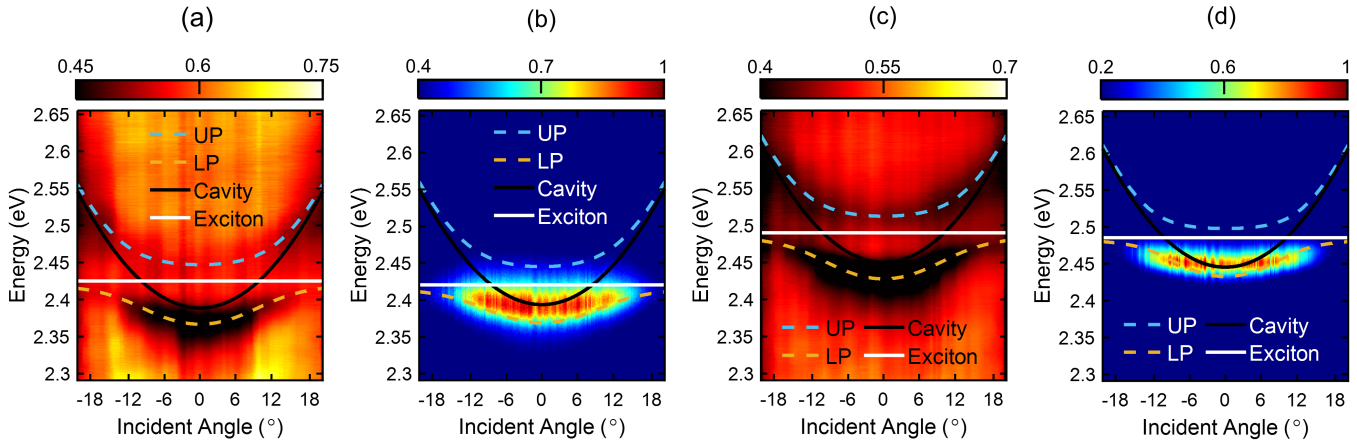

FIG. 5. Temperature-dependent angle-resolved measurements for cavities with similar detunings. (a–b) shows the angle-resolved reflectance and PL spectra with $\Delta E = -36.3$ meV and $\hbar\Omega_R = 71.58$ meV at T = 300 K. (c–d) shows the angle-resolved reflectance and PL spectra with $\Delta E = -39.8$ meV and $\hbar\Omega_R = 74.65$ meV at T = 5 K.

renormalize the polariton dispersion characteristics, leading to the blue-shifting of LP emission energies.

The temperature-dependent characteristics of polariton dispersion were also examined by measuring angle-resolved spectra of the NPL–cavity system at both room temperature (300 K) and cryogenic temperature (5 K) while maintaining a consistent detuning, as illustrated in Fig. 5. It should be noted that obtaining spectral measurements from the same spot at different temperatures changes the cavity–exciton detuning since the heavy-hole exciton energy blue-shifts ($\approx$ 68 meV blue-shift in PL was observed when the temperature was varied from 300 K to 5 K, see Fig. S6 in *Supplementary Information*) at lower temperatures.[70] Although the PL spectrum of these NPLs is found to be dominated by trion emission at low temperatures,[70] the cavity couples only to the heavy-hole excitons since the trions have negligible oscillator strength. This is validated by low-temperature absorbance measurements of NPL films where any sign of trion absorption feature is absent (Fig. S6).

Upon fitting the angular dispersion data, the Rabi splitting is found to be similar during temperature variations, with only a slight increase of approximately 3 meV as the temperature decreases from 300 K to 5 K. This is consistent with the recent observation for 4.5 ML CdSe NPLs that the oscillator strength of their heavy-hole exciton transition does not appreciably change in the temperature range of 3 K – 300 K.[30] As such, the Rabi splitting is expected to be unaffected by temperature variations as long as the coupling strength exceeds the exciton and the photon decay rates.

Such a relatively stable Rabi splitting across a range of temperatures minimizes the requirement for stringent temperature control, offering significant potential for controlling chemical reactions[54,71] and studying polariton-mediated energy transfer under room temperature conditions.[72] Additionally, the substantial Rabi splitting achieved in our NPL–cavity system creates a pathway to enhance polariton-driven chemistry,[63] as electron transfer rates start to become significant when the Rabi splitting reaches around 100 meV.[73]

V. CONCLUSION

We have discovered an NPL–optical microcavity system that exhibits substantial light–matter coupling at room temperature. The resulting polariton states exhibit a Rabi splitting of 74.6 meV at 300 K, which is unaffected by changes in the light–matter detuning. The measured angle-resolved optical spectra of the system show excellent agreement with state-of-the-art quantum dynamics simulations, thus providing important insights into the fundamental understanding of polariton photophysics. Interaction with the large reservoir of dark states significantly alters the population dynamics of the polaritons, which is manifested as a blue-shift of the polariton PL spectrum from absorption. The polariton bottleneck effect is also observed in the LP PL spectra as cavity resonance is tuned to smaller energies with respect to the heavy-hole exciton, due to the population depletion at small angles. Room-temperature operation of such a polaritonic system offers the feasibility to manipulate chemical reactions and realize real-world quantum applications.

SUPPLEMENTARY INFORMATION

See *Supplementary Information* for comprehensive insights into the synthesis of 4.5 ML CdSe NPLs, sample preparation, and experimental characterization.

ACKNOWLEDGMENTS

This work was supported by the National Science Foundation Award “CCI Phase 1: NSF Center for Quantum Electrodynamics for Selective Transformations (QuEST)" program under Grant number CHE-2124398. The work was performed in part at the Cornell NanoScale Facility, an NNCI member supported by NSF Grant NNCI-2025233 and Integrated

Nanosystems Center (URnano). ERK appreciates valuable discussions with Johan Runeson on the MASH method.

DATA AVAILABILITY STATEMENT

The data that support the findings of this study are available from the corresponding author upon reasonable request.

Appendix A: Details of Theoretical Simulations

The generalized Holstein–Tavis–Cummings (GHTC) Hamiltonian can be expressed as[49–52]

$$\hat{H}_{\mathrm{GHTC}} = \hat{H}_{\mathrm{NPL}} + \hat{H}_{\mathrm{ph}} + \hat{H}_{\mathrm{I}}, \tag{A1}$$

where $\hat{H}_{\mathrm{NPL}}$ describes the ground and heavy-hole (HH) exciton states of N independent NPLs, $\hat{H}_{\mathrm{ph}}$ is the Hamiltonian for the quantized Fabry–Pérot cavity modes, and $\hat{H}_{\mathrm{I}}$ describes the matter–cavity interactions (between $\hat{H}_{\mathrm{NPL}}$ and $\hat{H}_{\mathrm{ph}}$).

We use the single-excited subspace to describe the NPL–cavity wavefunction, where at most one matter or photon excitation is present. The matter Hamiltonian $\hat{H}_{\mathrm{NPL}}$ is modeled as a sum of N identical, non-interacting NPLs each with their own phonon bath. For $j = [1,N]$, each NPL is modeled as a two-level system, with ground state $|g_j\rangle$ with reference electronic energy $E_{\mathrm{g}} = 0$ and HH exciton state $|x_j\rangle$ with energy E_{x}. The collective matter state labels are $|\mathrm{G}\rangle$ and $|\mathrm{X}_j\rangle$ where $|\mathrm{G}\rangle \equiv |g_1, g_2, ...g_N\rangle$ is the ground state of N NPLs with reference electronic energy $E_{\mathrm{G}} = 0$ and $|\mathrm{X}_j\rangle \equiv |g_1, g_2, ...x_j, ...g_N\rangle$ is the single excited HH state of the NPLs (where the j_{th} NPL is in its HH exciton state) with energy E_{x}.

The NPL Hamiltonian is modeled as

$$\hat{H}_{\mathrm{NPL}} = \sum_{j=1}^{N} \hbar\omega_{\mathrm{x}} \hat{\sigma}_j^{\dagger}\hat{\sigma}_j + \hat{H}_{\mathrm{ep}}, \tag{A2}$$

where $\omega_{\mathrm{x}} = E_{\mathrm{x}}/\hbar$ is the frequency of the HH exciton state and $\hat{\sigma}_j$ is the lowering operator of the HH exciton state of the jth NPL. Further, $\hat{H}_{\mathrm{ep}}$ denotes the exciton–phonon coupling term

$$\hat{H}_{\mathrm{ep}} = \sum_{j=1}^{N}\sum_{\nu}\left[\frac{P_{\nu,j}^2}{2} + \frac{1}{2}\omega_{\nu,j}^2\left(R_{\nu,j} - \sqrt{\frac{2\hbar S_{\nu,j}}{\omega_{\nu,j}}}\hat{\sigma}_j^{\dagger}\hat{\sigma}_j\right)^2\right], \tag{A3}$$

where $P_{\nu,j}$ and $R_{\nu,j}$ are the momentum and position of the ν_{th} phonon mode in the j_{th} NPL, with a frequency of $\hbar\omega_{\nu,j}$ that are coupled to states $|\mathrm{X}_j\rangle$ with the Huang-Rhys factor $S_{\nu,j}$. The corresponding reorganization energy for each individual NPL (for any j) is

$$\lambda_{\mathrm{x}} = \sum_{\nu}\hbar\omega_{\nu,j}S_{\nu,j}. \tag{A4}$$

The relations between the reorganization energies and the Franck-Condon excitation energies are $E_{\mathrm{x}}^0 = E_{\mathrm{x}} + \lambda_{\mathrm{x}}$. The phonon bath parameters were modeled after a super-ohmic spectral density fitted from Ref. 74 with reorganization energy $\lambda_{\mathrm{x}} = 5$ meV.

The cavity mode Hamiltonian $\hat{H}_{\mathrm{ph}}$ is modeled as a sum of K photon modes with different in-plane wavevector components. For $k = [0, K-1]$, each photon mode in the single-excited subspace is a two-level system with ground state $|0_k\rangle$, which is the vacuum 0-photon Fock state with reference energy $E_{\mathrm{vac}} = 0$, and excited state $|1_k\rangle$, which is the 1-photon Fock state with energy E_k. The collective cavity mode state labels are $|\mathbf{0}\rangle$ and $|\mathbf{1}_k\rangle$ where $|\mathbf{0}\rangle \equiv |0_0, 0_1, ...0_{K-1}\rangle$ is the ground state of K cavity modes with reference energy $E_{\mathbf{0}} = 0$ and $|\mathbf{1}_k\rangle \equiv |0_0, 0_1, ...1_k, ...0_{K-1}\rangle$ is the single-excited cavity state (where the k_{th} cavity mode has 1 photon) with energy E_k.

The photonic Hamiltonian is expressed as

$$\hat{H}_{\mathrm{ph}} = \sum_{\mathbf{k}}\hbar\omega_{\mathbf{k}}\left(\hat{a}_{\mathbf{k}}^{\dagger}\hat{a}_{\mathbf{k}} + \frac{1}{2}\right), \tag{A5}$$

where $\omega_{\mathbf{k}} = E_k/\hbar$ is the frequency of the kth angular mode of the cavity and $\hat{a}_{\mathbf{k}}$ is the annihilation operator of the kth mode. The light–matter coupling term is expressed as

$$\hat{H}_{\mathrm{I}} = \sum_{j=1}^{N}\sum_{\mathbf{k}}\hbar\sqrt{N}g_{\mathrm{c}}(\hat{\sigma}_j^{\dagger}\hat{a}_{\mathbf{k}}e^{i\bar{\mathbf{r}}_j\cdot\mathbf{k}} + \hat{\sigma}_j\hat{a}_{\mathbf{k}}^{\dagger}e^{-i\bar{\mathbf{r}}_j\cdot\mathbf{k}}), \tag{A6}$$

where $\bar{\mathbf{r}}_j$ is the center-of-mass position of the j_{th} NPL, $\mathbf{k}$ is the wavevector of a cavity mode that satisfies Eq. (2), and $\sqrt{N}g_c$ is the light–matter coupling strength of the HH. Note that we have assumed each individual coupling strength between the cavity modes and each NPL to be identical.

The system wavefunction is confined to the zero and *single-excited subspace*. We label states in the combined NPL and cavity Hilbert space in a condensed fashion (e.g. $|\mathrm{X}_j\rangle \otimes |\mathbf{0}\rangle \equiv |\mathrm{X}_j, \mathbf{0}\rangle$). The dynamics of the GHTC model in the presence of cavity loss are propagated using the L-MASH method which incorporates Lindblad dissipative dynamics into the recently described multi-state mapping approach to surface hopping (MASH) method[47,48,75].

The polariton states $|\psi_n(R)\rangle$ in this GHTC model are the eigenstates of the polariton Hamiltonian $\hat{H}_{\mathrm{pl}} = \hat{H}_{\mathrm{GHTC}} - \sum_{\nu,j}P_{\nu,j}^2/2$ at nuclear configuration R

$$\hat{H}_{\mathrm{pl}}(R)|\psi_n(R)\rangle = E_n(R)|\psi_n(R)\rangle, \tag{A7}$$

where $E_n(R)$ is the energy of the n_{th} polariton state. In this polariton basis $\{|\psi_n(R)\rangle\}$, the system wavefunction $|\Psi(t)\rangle$ at time t can be written as

$$|\Psi(t)\rangle = \sum_n c_n(t)|\psi_n(R(t))\rangle, \tag{A8}$$

where $\{c_n(t)\}$ are the wavefunction expansion coefficients in the polariton basis. The elements of the reduced density matrix estimator $\rho(t)$ of MASH for a single trajectory can be written in terms of these coefficients as

$$\rho_{nm}(t) = \alpha_{\mathrm{N}}c_n(t)c_m^*(t) - |\beta_{\mathrm{N}}|\delta_{nm}, \tag{A9}$$

where $\alpha_{\mathrm{N}} = (\mathrm{N_s}-1)/(-1+\sum_{n=1}^{\mathrm{N_s}}1/n)$ and $\beta_{\mathrm{N}} = (1-\alpha_{\mathrm{N}})/\mathrm{N_s}$ are constants depending on the total number of states $\mathrm{N_s}$. The

constant $|\beta_N|$ acts as an effective zero-point energy for the populations. The full details on the implementation of multi-state MASH dynamics can be found in Ref. 48.

In addition to the above unitary time-evolution governed by $\hat{H}_{\mathrm{GHTC}}$, the effects of cavity loss and incoherent driving are incorporated into the dynamics through the L-MASH algorithm which allows for the efficient simulation of Lindblad dissipative dynamics at the wavefunction level. The dissipative part of the L-MASH algorithm is similar to that of the Lindblad mean-field Ehrenfest (L-MFE) method[76] except that the equations have been modified to account for $Z = |\beta_N|/\alpha_N$, the *normalized* effective zero-point energy of the populations. For Lindblad jump operators of the form $|0\rangle\langle 1|$, corresponding to an incoherent transition from state $|1\rangle$ to state $|0\rangle$, the L-MASH method modifies the wavefunction expansion coefficients of states $|1\rangle$ and $|0\rangle$ for a time step dt as

$$c_1(t+dt) = e^{i\theta_{r1}} e^{i\varphi_1} \sqrt{e^{-\Gamma dt}|c_1(t)|^2 + (1-e^{-\Gamma dt})Z}, \tag{A10a}$$

$$c_0(t+dt) = e^{i\theta_{r0}} e^{i\varphi_0} \sqrt{|c_0(t)|^2 + (1-e^{-\Gamma dt})(|c_1(t)|^2 - Z)}, \tag{A10b}$$

where Γ is the jump operator strength (i.e. the decay/pumping rate), φ_0 and φ_1 are the complex phases of $c_0(t)$ and $c_1(t)$, respectively, and θ_{r0} and θ_{r1} are the phases randomly sampled from the uniform probability distributions

$$\mathscr{P}(\theta_{ri}) = \frac{1}{2\Delta\theta_{ri}}, \quad -\Delta\theta_{ri} \le \theta_{ri} < \Delta\theta_{ri}, \quad i = 0,1 \tag{A11}$$

with distribution widths $\Delta\theta_{r0}$ and $\Delta\theta_{r1}$ determined from the following transcendental equations

$$\frac{\sin(\Delta\theta_{r1})}{\Delta\theta_{r1}} = \frac{e^{-\Gamma dt/2}|c_1(t)|}{\sqrt{e^{-\Gamma dt}|c_1(t)|^2 + (1-e^{-\Gamma dt})Z}}, \tag{A12a}$$

$$\frac{\sin(\Delta\theta_{r0})}{\Delta\theta_{r0}} = \frac{|c_0(t)|}{\sqrt{|c_0(t)|^2 + (1-e^{-\Gamma dt})(|c_1(t)|^2 - Z)}}. \tag{A12b}$$

Note that for methods where the effective zero-point energy $Z = 0$, the dissipative equations A10-A12 simplify to those of the L-MFE method[76].

The combination of the GHTC and stochastic Lindblad dissipation propagation for the system-reduced density matrix can be written as

$$\hat{\rho}(t+\mathrm{d}t) = e^{\mathscr{L}dt}[\hat{\rho}(t)] = e^{\mathscr{L}_{\hat{L}}\mathrm{d}t} e^{\mathscr{L}_{\hat{H}}\mathrm{d}t} \hat{\rho}(t), \tag{A13}$$

where $e^{\mathscr{L}_{\hat{H}}\mathrm{d}t}$ is the GHTC propagation for nuclear time step dt and $e^{\mathscr{L}_{\hat{L}}\mathrm{d}t}$ is the dissipative propagation from Eq. A10 for the jump operators. In this work, we use jump operators in the polariton basis. The jump operators $\{|\mathrm{G},\mathbf{0}\rangle\langle\psi_n|\}$ correspond to cavity loss from polariton state $n \ge 1$ with loss rate $\Gamma_{c,n} = \gamma_c \sum_k |\langle \mathrm{G}, \mathbf{1}_k|\psi_n\rangle|^2$ where γ_c is the bare cavity loss rate. The jump operators $\{|\psi_n\rangle\langle \mathrm{G},\mathbf{0}|\}$ correspond to incoherent driving from the ground state to polariton state $n \ge 1$ with pump rate $\Gamma_{x,n} = \gamma_x \sum_j |\langle \mathrm{X}_j, \mathbf{0}|\psi_n\rangle|^2$ where γ_x is the bare exciton pump rate.

The initial conditions for the simulation are $\hat{\rho}(0) = \hat{\rho}_{\mathbf{R}} \otimes |\mathrm{G},\mathbf{0}\rangle\langle \mathrm{G},\mathbf{0}|$, where $\hat{\rho}_{\mathbf{R}}$ is the initial nuclear density operator. The positions and momenta of the phonon modes are sampled from a Wigner distribution of the nuclear density operator $\hat{\rho}_{\mathbf{R}}$ as follows

$$(\hat{\rho}_{\mathbf{R}})^W \propto \Pi_{\nu,j} \exp\Big[-\tanh\Big(\frac{\omega_{\nu,j}}{2k_B T}\Big)\cdot\Big(\omega_{\nu,j}R_{\nu,j}^2 + \frac{P_{\nu,j}^2}{\omega_{\nu,j}}\Big)\Big], \tag{A14}$$

with temperature $T = 300$ K.

In this work, to keep the computational expense tractable, we use $N = 160 > K = 40$ and scale the individual coupling strength g_c to match the fitted Rabi splitting through the relation $\hbar\Omega_R = 2\sqrt{N}g_c$. The bare cavity loss rate was set to $\gamma_c = \omega_c/Q$ with $Q = 60$. The bare exciton pump rate was set to $\hbar\gamma_x = 6/N$ meV. The dynamics were simulated for a total time of 2 ps with a timestep $dt = 0.5$ fs. The angle-resolved photoluminescence (PL) spectra at steady state time $t_{ss} = 2$ ps for energy E and in-plane wavevector index k was calculated as

$$\mathrm{PL}(E,k) = \sum_n \frac{|c_n(t_{ss})|^2 |\langle \mathrm{G}, \mathbf{1}_k|\psi_n\rangle|^2 \Gamma_{c,n}/2}{(E-E_n)^2 + (\Gamma_{c,n}/2)^2}. \tag{A15}$$

The PL spectrum was averaged over 10,000 trajectories.

REFERENCES

[1] J. Wen, H. Wang, W. Wang, Z. Deng, C. Zhuang, Y. Zhang, F. Liu, J. She, J. Chen, H. Chen, *et al.*, "Room-temperature strong light–matter interaction with active control in single plasmonic nanorod coupled with two-dimensional atomic crystals," Nano letters **17**, 4689–4697 (2017).

[2] S. Ghosh, R. Su, J. Zhao, A. Fieramosca, J. Wu, T. Li, Q. Zhang, F. Li, Z. Chen, T. Liew, *et al.*, "Microcavity exciton polaritons at room temperature," Photonics Insights **1**, R04–R04 (2022).

[3] Y. Chen, D. Sharp, A. Saxena, H. Nguyen, B. M. Cossairt, and A. Majumdar, "Integrated quantum nanophotonics with solution-processed materials," Advanced Quantum Technologies **5**, 2100078 (2022).

[4] D. E. Chang, V. Vuletić, and M. D. Lukin, "Quantum nonlinear optics—photon by photon," Nature Photonics **8**, 685–694 (2014).

[5] L.-M. Duan and H. Kimble, "Scalable photonic quantum computation through cavity-assisted interactions," Physical review letters **92**, 127902 (2004).

[6] I. Carusotto and C. Ciuti, "Quantum fluids of light," Reviews of Modern Physics **85**, 299 (2013).

[7] W. Hu, I. Gustin, T. D. Krauss, and I. Franco, "Tuning and enhancing quantum coherence time scales in molecules via light-matter hybridization," The Journal of Physical Chemistry Letters **13**, 11503–11511 (2022).

[8] E. Rozas, M. Martín, C. Tejedor, L. Viña, G. Deligeorgis, Z. Hatzopoulos, and P. Savvidis, "Temperature dependence of the coherence in polariton condensates," Physical Review B **97**, 075442 (2018).

[9] K. Hao, G. Moody, F. Wu, C. K. Dass, L. Xu, C.-H. Chen, L. Sun, M.-Y. Li, L.-J. Li, A. H. MacDonald, *et al.*, "Direct measurement of exciton valley coherence in monolayer wse2," Nature Physics **12**, 677–682 (2016).

[10] D. Sanvitto and S. Kéna-Cohen, "The road towards polaritonic devices," Nature materials **15**, 1061–1073 (2016).

[11] T. Volz, A. Reinhard, M. Winger, A. Badolato, K. J. Hennessy, E. L. Hu, and A. Imamoğlu, "Ultrafast all-optical switching by single photons," Nature Photonics **6**, 605–609 (2012).

[12] W. Chen, K. M. Beck, R. Bücker, M. Gullans, M. D. Lukin, H. Tanji-Suzuki, and V. Vuletić, "All-optical switch and transistor gated by one stored photon," Science **341**, 768–770 (2013).

[13] R. Su, J. Wang, J. Zhao, J. Xing, W. Zhao, C. Diederichs, T. C. Liew, and Q. Xiong, "Room temperature long-range coherent exciton polariton condensate flow in lead halide perovskites," Science advances **4**, eaau0244 (2018).

[14] R. Su, S. Ghosh, J. Wang, S. Liu, C. Diederichs, T. C. Liew, and Q. Xiong, "Observation of exciton polariton condensation in a perovskite lattice at room temperature," Nature Physics **16**, 301–306 (2020).

[15] J. Wu, S. Ghosh, R. Su, A. Fieramosca, T. C. Liew, and Q. Xiong, "Nonlinear parametric scattering of exciton polaritons in perovskite microcavities," Nano Letters **21**, 3120–3126 (2021).

[16] Z. Zhen, S.-Y. Jin, R. Jie, H.-Y. Liang, and X.-S. Xu, "Strong coupling between colloidal quantum dots and a microcavity with hybrid structure at room temperature," Photonics Research **10**, 913–921 (2022).

[17] D. Dovzhenko, M. Lednev, K. Mochalov, I. Vaskan, P. Samokhvalov, Y. Rakovich, and I. Nabiev, "Strong exciton- photon coupling with colloidal quantum dots in a tunable microcavity," Applied Physics Letters **119** (2021).

[18] K. Peng and E. Rabani, "Polaritonic bottleneck in colloidal quantum dots," Nano Letters **23**, 10587–10593 (2023).

[19] N. C. Giebink, G. P. Wiederrecht, and M. R. Wasielewski, "Strong exciton-photon coupling with colloidal quantum dots in a high-q bilayer microcavity," Applied Physics Letters **98** (2011).

[20] X. Xu and S. Jin, "Strong coupling of single quantum dots with low-refractive-index/high-refractive-index materials at room temperature," Science advances **6**, eabb3095 (2020).

[21] K. Gong, Y. Zeng, and D. F. Kelley, "Extinction coefficients, oscillator strengths, and radiative lifetimes of cdse, cdte, and cdte/cdse nanocrystals," The Journal of Physical Chemistry C **117**, 20268–20279 (2013).

[22] S. Ithurria and B. Dubertret, "Quasi 2d colloidal cdse platelets with thicknesses controlled at the atomic level," Journal of the American Chemical Society **130**, 16504–16505 (2008).

[23] S. Ithurria, M. Tessier, B. Mahler, R. Lobo, B. Dubertret, and A. L. Efros, "Colloidal nanoplatelets with two-dimensional electronic structure," Nat. Mater. **10**, 936–941 (2011).

[24] M. D. Tessier, C. Javaux, I. Maksimovic, V. Loriette, and B. Dubertret, "Spectroscopy of single cdse nanoplatelets," ACS nano **6**, 6751–6758 (2012).

[25] J. M. Winkler, F. T. Rabouw, A. A. Rossinelli, S. V. Jayanti, K. M. McPeak, D. K. Kim, B. Le Feber, F. Prins, and D. J. Norris, "Room-temperature strong coupling of cdse nanoplatelets and plasmonic hole arrays," Nano letters **19**, 108–115 (2018).

[26] I. Shlesinger, H. Monin, J. Moreau, J.-P. Hugonin, M. Dufour, S. Ithurria, B. Vest, and J.-J. Greffet, "Strong coupling of nanoplatelets and surface plasmons on a gold surface," ACS Photonics **6**, 2643–2648 (2019).

[27] M. Oda, K. Yamato, J. Egashira, and H. Kondo, "Room-temperature strong coupling of hexane-dispersed colloidal cdse nanoplatelets in a microcavity composed of two bragg reflectors," arXiv preprint arXiv:2309.04743 (2023).

[28] M. L. Steigerwald and L. E. Brus, "Semiconductor crystallites: A class of large molecules," Acc. Chem. Res. **23**, 183–188 (1990).

[29] Y. Gao, M. C. Weidman, and W. A. Tisdale, "Cdse nanoplatelet films with controlled orientation of their transition dipole moment," Nano Letters **17**, 3837–3843 (2017).

[30] B. T. Diroll and R. D. Schaller, "Reexamination of the giant oscillator strength effect in cdse nanoplatelets," The Journal of Physical Chemistry C **127**, 4601–4608 (2023).

[31] L. C. Flatten, S. Christodoulou, R. K. Patel, A. Buccheri, D. M. Coles, B. P. Reid, R. A. Taylor, I. Moreels, and J. M. Smith, "Strong exciton–photon coupling with colloidal nanoplatelets in an open microcavity," Nano Letters **16**, 7137–7141 (2016).

[32] L. Qiu, A. Mandal, O. Morshed, M. T. Meidenbauer, W. Girten, P. Huo, A. N. Vamivakas, and T. D. Krauss, "Molecular polaritons generated from strong coupling between cdse nanoplatelets and a dielectric optical cavity," The Journal of Physical Chemistry Letters **12**, 5030–5038 (2021).

[33] B. Li, S. Zu, Z. Zhang, L. Zheng, Q. Jiang, B. Du, Y. Luo, Y. Gong, Y. Zhang, F. Lin, *et al.*, "Large rabi splitting obtained in ag-ws2 strong-coupling heterostructure with optical microcavity at room temperature," Opto-Electronic Advances **2**, 190008 (2019).

[34] A. Mandal, M. A. Taylor, B. M. Weight, E. R. Koessler, X. Li, and P. Huo, "Theoretical advances in polariton chemistry and molecular cavity quantum electrodynamics," Chemical Reviews **123**, 9786–9879 (2023).

[35] P. Törmä and W. L. Barnes, "Strong coupling between surface plasmon polaritons and emitters: a review," Reports on Progress in Physics **78**, 013901 (2014).

[36] D. G. Lidzey, D. Bradley, M. Skolnick, T. Virgili, S. Walker, and D. Whittaker, "Strong exciton–photon coupling in an organic semiconductor microcavity," Nature **395**, 53–55 (1998).

[37] V. Savona, "Fifteen years of microcavity polaritons," The Physics of Semiconductor Microcavities (2007).

[38] W. Chiang, O. Morshed, and T. Krauss, *Quantum Confined Semiconductor Nanocrystals* (American Chemical Society, 2023).

[39] M. Tavis and F. W. Cummings, "Exact solution for an n-molecule—radiation-field hamiltonian," Physical Review **170**, 379 (1968).

[40] G. Khitrova, H. Gibbs, M. Kira, S. W. Koch, and A. Scherer, "Vacuum rabi splitting in semiconductors," Nature physics **2**, 81–90 (2006).

[41] A. A. Rossinelli, A. Riedinger, P. Marqués-Gallego, P. N. Knüsel, F. V. Antolinez, and D. J. Norris, "High-temperature growth of thick-shell cdse/cds core/shell nanoplatelets," Chemical communications **53**, 9938–9941 (2017).

[42] M. I. Vasilevskiy, D. G. Santiago-Pérez, C. Trallero-Giner, N. M. Peres, and A. Kavokin, "Exciton polaritons in two-dimensional dichalcogenide layers placed in a planar microcavity: Tunable interaction between two bose-einstein condensates," Physical Review B **92**, 245435 (2015).

[43] D. Lidzey, D. Bradley, T. Virgili, A. Armitage, M. Skolnick, and S. Walker, "Room temperature polariton emission from strongly coupled organic semiconductor microcavities," Physical review letters **82**, 3316 (1999).

[44] P. Geiregat, C. Rodá, I. Tanghe, S. Singh, A. Di Giacomo, D. Lebrun, G. Grimaldi, J. Maes, D. Van Thourhout, I. Moreels, *et al.*, "Localization-limited exciton oscillator strength in colloidal cdse nanoplatelets revealed by the optically induced stark effect," Light: Science & Applications **10**, 112 (2021).

[45] J. Fregoni, F. J. Garcia-Vidal, and J. Feist, "Theoretical challenges in polaritonic chemistry," ACS photonics **9**, 1096–1107 (2022).

[46] J. A. Campos-Gonzalez-Angulo, R. F. Ribeiro, and J. Yuen-Zhou, "Resonant catalysis of thermally activated chemical reactions with vibrational polaritons," Nature communications **10**, 4685 (2019).

[47] M. Amin, E. R. Koessler, O. Morshed, F. Awan, N. M. Cogan, R. Collison, W. Girten, C. S. Leiter, A. N. Vamivakas, P. Huo, and T. D. Krauss, "Long-lived dynamics enables exciton-polariton upconversion in cdse nanoplatelets," ChemRxiv (2023), 10.26434/chemrxiv-2023-4tshv.

[48] J. E. Runeson and D. E. Manolopoulos, "A multi-state mapping approach to surface hopping," J. Chem. Phys. **159**, 094115 (2023).

[49] A. Mandal, M. A. Taylor, B. M. Weight, E. R. Koessler, X. Li, and P. Huo, "Theoretical advances in polariton chemistry and molecular cavity quantum electrodynamics," Chemical Reviews **123**, 9786–9879 (2023).

[50] R. H. Tichauer, J. Feist, and G. Groenhof, "Multi-scale dynamics simulations of molecular polaritons: The effect of multiple cavity modes on polariton relaxation," J. Chem. Phys. **154**, 104112 (2021).

[51] K. B. Arnardottir, A. J. Moilanen, A. Strashko, P. Törmä, and J. Keeling, "Multimode organic polariton lasing," Phys. Rev. Lett. **125**, 233603 (2020).

[52] A. M. Berghuis, R. H. Tichauer, L. M. A. de Jong, I. Sokolovskii, P. Bai, M. Ramezani, S. Murai, G. Groenhof, and J. G. Rivas, "Controlling exciton propagation in organic crystals through strong coupling to plasmonic nanoparticle arrays," ACS Photonics **9**, 2263–2272 (2022).

[53] T. E. Li, A. Nitzan, and J. E. Subotnik, "Polariton relaxation under vibrational strong coupling: Comparing cavity molecular dynamics simulations against fermi's golden rule rate," The Journal of Chemical Physics **156** (2022).

[54] F. Herrera and J. Owrutsky, "Molecular polaritons for controlling chemistry with quantum optics," The Journal of chemical physics **152** (2020).

[55] C. López, H. Christ, J. Retamal, and E. Solano, "Effective quantum dynamics of interacting systems with inhomogeneous coupling," Physical Review A **75**, 033818 (2007).

[56] F. Spano, "Optical microcavities enhance the exciton coherence length and eliminate vibronic coupling in j-aggregates," The Journal of Chemical Physics **142** (2015).

[57] F. Herrera and F. C. Spano, "Cavity-controlled chemistry in molecular ensembles," Physical Review Letters **116**, 238301 (2016).

[58] F. Fassioli, K. H. Park, S. E. Bard, and G. D. Scholes, "Femtosecond photo-

physics of molecular polaritons," The Journal of Physical Chemistry Letters **12**, 11444–11459 (2021).
[59]G. D. Scholes, C. A. DelPo, and B. Kudisch, "Entropy reorders polariton states," The Journal of Physical Chemistry Letters **11**, 6389–6395 (2020).
[60]B. Xiang, R. F. Ribeiro, L. Chen, J. Wang, M. Du, J. Yuen-Zhou, and W. Xiong, "State-selective polariton to dark state relaxation dynamics," The Journal of Physical Chemistry A **123**, 5918–5927 (2019).
[61]D. M. Coles, P. Michetti, C. Clark, A. M. Adawi, and D. G. Lidzey, "Temperature dependence of the upper-branch polariton population in an organic semiconductor microcavity," Physical Review B **84**, 205214 (2011).
[62]F. C. Spano, "The spectral signatures of frenkel polarons in h-and j-aggregates," Accounts of chemical research **43**, 429–439 (2010).
[63]R. F. Ribeiro, L. A. Martínez-Martínez, M. Du, J. Campos-Gonzalez-Angulo, and J. Yuen-Zhou, "Polariton chemistry: controlling molecular dynamics with optical cavities," Chemical science **9**, 6325–6339 (2018).
[64]N. Shammah, N. Lambert, F. Nori, and S. De Liberato, "Superradiance with local phase-breaking effects," Physical Review A **96**, 023863 (2017).
[65]R. Bhuyan, J. Mony, O. Kotov, G. W. Castellanos, J. Gomez Rivas, T. O. Shegai, and K. Borjesson, "The rise and current status of polaritonic photochemistry and photophysics," Chemical Reviews (2023).
[66]F. Tassone, C. Piermarocchi, V. Savona, A. Quattropani, and P. Schwendimann, "Bottleneck effects in the relaxation and photoluminescence of microcavity polaritons," Physical Review B **56**, 7554 (1997).
[67]M. Laitz, A. E. Kaplan, J. Deschamps, U. Barotov, A. H. Proppe, I. García-Benito, A. Osherov, G. Grancini, D. W. deQuilettes, K. A. Nelson, *et al.*, "Uncovering temperature-dependent exciton-polariton relaxation mechanisms in hybrid organic-inorganic perovskites," Nature Communications **14**, 2426 (2023).
[68]Y. Sun, Y. Yoon, M. Steger, G. Liu, L. N. Pfeiffer, K. West, D. W. Snoke, and K. A. Nelson, "Direct measurement of polariton–polariton interaction strength," Nature Physics **13**, 870–875 (2017).
[69]S. Utsunomiya, L. Tian, G. Roumpos, C. Lai, N. Kumada, T. Fujisawa, M. Kuwata-Gonokami, A. Löffler, S. Höfling, A. Forchel, *et al.*, "Observation of bogoliubov excitations in exciton-polariton condensates," Nature Physics **4**, 700–705 (2008).
[70]A. F. Vong, S. Irgen-Gioro, Y. Wu, and E. A. Weiss, "Origin of low temperature trion emission in cdse nanoplatelets," Nano letters **21**, 10040–10046 (2021).
[71]J. A. Hutchison, T. Schwartz, C. Genet, E. Devaux, and T. W. Ebbesen, "Modifying chemical landscapes by coupling to vacuum fields," Angewandte Chemie International Edition **51**, 1592–1596 (2012).
[72]D. M. Coles, N. Somaschi, P. Michetti, C. Clark, P. G. Lagoudakis, P. G. Savvidis, and D. G. Lidzey, "Polariton-mediated energy transfer between organic dyes in a strongly coupled optical microcavity," Nature materials **13**, 712–719 (2014).
[73]A. Mandal, T. D. Krauss, and P. Huo, "Polariton-mediated electron transfer via cavity quantum electrodynamics," The Journal of Physical Chemistry B **124**, 6321–6340 (2020).
[74]D. Jasrasaria and E. Rabani, "Circumventing the phonon bottleneck by multiphonon-mediated hot exciton cooling at the nanoscale," npj Comput Mater **9**, 145 (2023).
[75]J. R. Mannouch and J. O. Richardson, "A mapping approach to surface hopping," J. Chem. Phys. **158**, 104111 (2023).
[76]E. R. Koessler, A. Mandal, and P. Huo, "Incorporating Lindblad decay dynamics into mixed quantum-classical simulations," The Journal of Chemical Physics **157**, 064101 (2022).